

# Ferroelectrically tunable magnetic and topological multistates in thin films of $\text{MnBi}_2\text{Te}_4$ family

Guoliang Yu,<sup>1</sup> Chuhan Tang,<sup>1</sup> Zhiqiang Tian,<sup>1</sup> Ziming Zhu,<sup>1</sup> Anlian Pan,<sup>2</sup> Mingxing Chen,<sup>1,\*</sup> and Xingqiu Chen<sup>3,4</sup>

<sup>1</sup>Key Laboratory for Matter Microstructure and Function of Hunan Province,  
Key Laboratory of Low-Dimensional Quantum Structures and Quantum Control of Ministry of Education,  
School of Physics and Electronics, Hunan Normal University, Changsha 410081, China

<sup>2</sup>Key Laboratory for Micro-Nano Physics and Technology of Hunan Province,  
College of Materials Science and Engineering, Hunan University, Changsha 410082, China

<sup>3</sup>Shenyang National Laboratory for Materials Science, Institute of Metal Research,  
Chinese Academy of Sciences, 110016 Shenyang, People's Republic of China.

<sup>4</sup>School of Materials Science and Engineering, University of Science and  
Technology of China, 110016 Shenyang, People's Republic of China.

(Dated: January 4, 2023)

Ferroelectric control of two-dimensional magnetism is promising in fabricating electronic devices with high speed and low energy consumption. The newly discovered layered  $\text{MnBi}_2\text{Te}_4(\text{Bi}_2\text{Te}_3)_n$  and their Sb counterparts exhibit A-type antiferromagnetism with intriguing topological properties. Here, we propose to obtain tunable magnetic multistates in their thin films by ferroelectrically manipulating the interlayer magnetic couplings (IMCs) based on the Heisenberg model and first-principles calculations. Our strategy relies on that interfacing the thin films with appropriate ferroelectric materials can switch on/off an interlayer hopping channel between Mn- $e_g$  orbitals as the polarizations reversed, thus resulting in a switchable interlayer antiferromagnetism-to-ferromagnetism transition. On the other hand, the interface effect leads to asymmetric energy barrier heights for the two polarization states. These properties allow us to build ferroelectrically switchable triple and quadruple magnetic states with multiple Chern numbers in thin films. Our study reveals that ferroelectrically switchable magnetic and topological multistates in  $\text{MnBi}_2\text{Te}_4$  family can be obtained by rational design for multifunctional electronic devices, which can also be applied to other two-dimensional magnetic materials.

## I. INTRODUCTION

Two-dimensional (2D) magnetic materials provide an ideal platform to explore novel magnetic and electronic properties<sup>1-7</sup>. The delicate interlayer exchange couplings in these systems enable a variety of methods of manipulating their magnetism. For instance, recent studies revealed that the A-type antiferromagnetic (AFM)  $\text{CrI}_3$  bilayer could be tuned into ferromagnetic (FM) by external electric field<sup>8,9</sup>, electrostatic doping<sup>10,11</sup>, and interface engineering<sup>12-17</sup>. Twisting the bilayer may yield non-collinear magnetism<sup>18-20</sup>.

Recently, the  $\text{MnBi}_2\text{Te}_4$  family, i.e.,  $\text{MnBi}_2\text{Te}_4(\text{Bi}_2\text{Te}_3)_n$  and  $\text{MnSb}_2\text{Te}_4(\text{Bi}_2\text{Te}_3)_n$ , which are hereafter referred to as MAT, have much great attention due to the coexistence and interesting interplay of intrinsic magnetism and band topology in them<sup>21-38</sup>. This series of materials also have a layered van der Waals (vdW) structure with an A-type AFM structure as revealed by experiments<sup>39-42</sup>, which preserves the combination of the time-reversal and a half lattice translation symmetry. As a result, many of them show nontrivial topological properties such as topological insulators<sup>21</sup> and axion insulators<sup>22</sup>. Moreover, the systems can be turned into Weyl semimetals as the interlayer couplings become ferromagnetic<sup>22,23,36</sup>.

The A-type AFM coupling in MAT yields unusual even-odd layer-number dependent magnetism for their thin films<sup>35,43,44</sup>. The even-number (even- $N$ ) systems are

expected to have no net magnetization. Whereas those with odd-number (odd- $N$ ) layers have uncompensated magnetization. This difference can lead to distinct topological properties for them. For instance, the thin films of  $\text{MnBi}_2\text{Te}_4$  with odd- $N$  septuple layers are quantum anomalous Hall insulators. However, those with even- $N$  layers have a zero Chern number<sup>43</sup>. Instead, their topological properties can be characterized by the so-called pseudospin Chern number<sup>45</sup>. Due to the weak interlayer interaction, small magnetic fields could induce spin-flip transitions, giving rise to an AFM-to-FM transition in the IMCs<sup>35,41</sup>. Chemical dopings<sup>46,47</sup> and antisite defects<sup>48-52</sup> can also be used to manipulate the IMCs in these systems, although they may complicate the nature of the surface states. First-principles calculations suggest that the AFM double-septuple  $\text{MnBi}_2\text{Te}_4$  could be driven into a Chern insulator with a high Chern number under electric fields<sup>53</sup>.

In this Letter, we propose to ferroelectrically tune the IMCs in  $\text{MnBi}_2\text{Te}_4$  thin films for magnetic multistates by interface, which is desired for memory devices with high density storage, high speed, and low power consumption. We reveal that hole doping can lead to an interlayer AFM-to-FM transition in MAT bilayers based on the understanding of the IMCs using the Heisenberg model. We provide a guideline for designing ferroelectric substrates that may induce transitions in the interlayer exchange couplings, i.e., polarization dependent IMCs, as demonstrated by our first-principles calculations. Moreover, we

find that the interface effect results in symmetry breaking in the two polarization states of the FE substrate. This asymmetry allows us to design switchable magnetic multistates in sandwich structures made of  $\text{MnBi}_2\text{Te}_4$  multilayers and 2D ferroelectric (FE) materials, which also exhibit distinct electronic and topological properties.

We begin by presenting the concept of FE tuning of IMCs in MAT bilayers, which is shown in Fig. 1. In these systems, each Mn atom is coordinated with six chalcogen atoms, which form a distorted octahedron. The Mn-3d orbitals are split into triply degenerate  $t_{2g}$  states and the doubly degenerate  $e_g$  states due to the octahedral ligand field. The states are further split due to the magnetic exchange interaction between the Mn atoms. As a result, the majority states of the  $t_{2g}$  and  $e_g$  orbitals are fully occupied by the five  $d$  electrons of the  $\text{Mn}^{2+}$  ions (see Fig. 1), resulting in a high spin state for the  $\text{Mn}^{2+}$  ions. Like the 2D magnetic bilayers reported by Refs 31 and 54, this type of occupation favors AFM IMCs between the  $\text{Mn}^{2+}$  ions, which are mediated by the  $p$ -orbitals of the nonmetallic atoms (denoted by  $\{p\dots p\}$ ). Whereas FM IMCs are energetically unfavorable because the  $e_g^\uparrow - \{p\dots p\} - e_g^\uparrow$  hopping between the Mn- $d$  orbitals of adjacent layers is prohibited<sup>31,54,55</sup>. For our systems, reducing the occupation of the  $d$  orbitals makes the  $e_g^\uparrow - \{p\dots p\} - e_g^\uparrow$  hopping channel energetically favorable, thus enhancing the stability of the FM IMCs. Indeed, our DFT calculations indicate that all the MAT bilayers undergo the AFM-to-FM transition by small hole dopings (see Fig. 1c and Fig. S1), which is also expected for their multilayers.

The IMCs in MAT-2L can be understood using the following spin Hamiltonian.

$$H = \sum_{i,j} J_{\parallel}^t \mathbf{S}_i \cdot \mathbf{S}_j + \sum_{m,n} J_{\parallel}^b \mathbf{S}_m \cdot \mathbf{S}_n + \sum_{i,m} J_{\perp} \mathbf{S}_i \cdot \mathbf{S}_m, \quad (1)$$

where  $J_{\parallel}$  and  $J_{\perp}$  denote the intra- and interlayer exchange interactions between the Mn ions, respectively. The intralayer ones are denoted by  $J_{\parallel}^t$  for the top layer and  $J_{\parallel}^b$  for the bottom layer, for which only the first nearest-neighbor interactions are taken into account.  $J_{\parallel}^t$  are equal to  $J_{\parallel}^b$  for the freestanding MAT-2L. Whereas for the interlayer ones, the second nearest neighbors are included. For the bilayers without doping, we obtain positive  $J_{\perp}^{1st}$  and negative  $J_{\perp}^{2nd}$  (see Fig. 1d, Fig. S2 and Table S1). Note that the magnitude of  $J_{\perp}^{1st}$  is larger than that of  $J_{\perp}^{2nd}$ . So, the sum of  $J_{\perp}^{1st}$  and  $J_{\perp}^{2nd}$ , i.e.,  $\bar{J}_{\perp} = J_{\perp}^{1st} + J_{\perp}^{2nd}$ , is positive, which gives rise to AFM IMCs. Introducing hole doping suppresses  $J_{\perp}^{1st}$  while enhances  $J_{\perp}^{2nd}$ . As a result,  $\bar{J}_{\perp}$  decreases with increasing of the hole doping and eventually changes its sign across the AFM-to-FM transition (see Fig. 1d).

The hole doping over the MAT bilayers can be achieved via interfacial charge transfer which requires suitable band alignments between them and the substrates. When their bands are in the type-I or type-II alignment, interfacial charge transfer can be negligible. In

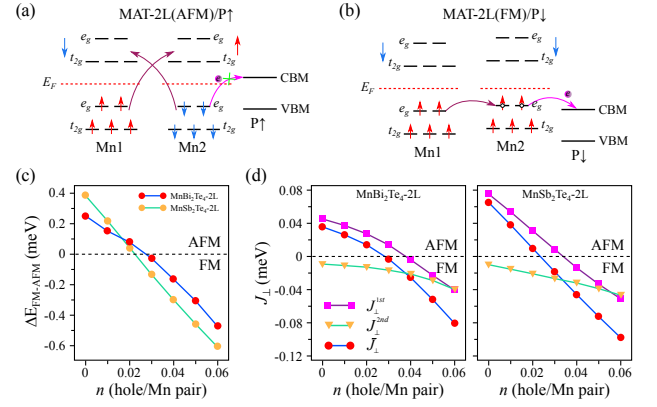


FIG. 1. Interface engineering of the IMCs in MAT bilayers. (a) Spin states of Mn ions for the AFM interlayer coupling. In the presence of a substrate that has a type-I or type-II band alignment with the bilayer, the IMCs remain AFM. (b) The IMCs becomes FM when there is a type-III band alignment between them so that the CBM of the substrate lower than the VBM of the MAT bilayer. In (b), the white circles denote hole dopings to the Mn- $e_g$  orbital. In (a, b), arrows denote spins. The dark and light red curves with an arrow denote electron hoppings are prohibited. We use a FE material as the substrate, whose polarizations are labeled by  $P$ .  $P \uparrow$  and  $P \downarrow$  represent the up and down polarizations, respectively. (c) Energy difference between the FM and AFM states as a function of hole doping for freestanding  $\text{MnBi}_2\text{Te}_4$  and  $\text{MnSb}_2\text{Te}_4$  bilayers.  $\Delta E = E_{FM} - E_{AFM}$ . (d) Doping dependence of  $J_{\perp}$  for the two systems.  $\bar{J}_{\perp} = J_{\perp}^{1st} + J_{\perp}^{2nd}$ .

these cases, the IMCs are most likely to be AFM. In contrast, electrons will be transferred from the MAT bilayer to the substrate when they are in the type-III band alignment that the valence band maximum (VBM) of the MAT bilayer are higher than the conduction band minimum (CBM) of the substrate. Namely, hole doping is introduced to the MAT bilayer, which is desired for the AFM-to-FM transition. Ferroelectrically switchable IMCs may be achieved if a 2D FE materials serves as the substrate so that reversing its polarizations gives rise to a switching of the band alignment from type-III to type-I (II) or vice versa (see Fig. 1). However, one can expect that the transferred electrons mainly come from the interfacial MAT layer because of the vdW-type interlayer bonding. Therefore, the spin-flipping most likely happen to the interfacial MAT layer rather than those further away from the substrate.

We now come to first-principles calculations of the heterostructures of MAT thin films and 2D FE materials, which were performed using the Vienna Ab initio Simulation Package<sup>56</sup>. We choose  $\text{In}_2\text{Se}_3$  monolayer as the substrate, which has been experimentally proved since its prediction in 2017<sup>57-59</sup>. Their heterostructures are built by slightly adjusting the lattice of  $\text{In}_2\text{Se}_3$  (The lattice mismatch between them is small). The pseudopotentials were constructed by the projector augmented wave method<sup>60,61</sup>. An  $11 \times 11 \times 1$  and  $21 \times 21 \times 1$   $\Gamma$ -

centered  $k$ -mesh were used to sample the 2D Brillouin zone for structural relaxation and electronic structure calculations, respectively. The plane-wave energy cutoff is set to 400 eV for all calculations. A 20 Å vacuum region was used between adjacent plates to avoid the interaction between neighboring periodic images. Van der Waals (vdW) dispersion forces between the adsorbate and the substrate were accounted for through the DFT-D3<sup>62</sup>. Different vdW methods/functionals such as DFT-D2 and optPBE-vdW were also used for comparison<sup>63–65</sup>. The systems were fully relaxed until the residual force on each atom is less than 0.01 eV/Å. The DFT+U method<sup>66</sup> is used to treat electron correlations due to the partially filled  $d$ -orbital of Mn for which a value of 5.34 eV is used<sup>21</sup>. Our results on the structural properties, magnetism, and band structures of the free-standing MAT films are consistent with previous studies<sup>21,32,36</sup>. The kinetic pathways of transitions between different polarization states are calculated using the climbing image nudge elastic band (CI-NEB) method<sup>67,68</sup>. The topological properties calculations were done using the WANNIER90<sup>69</sup> and WannierTools package<sup>70</sup>.

We have performed careful calculations over a number of stacking configurations (see Fig. S3, and Table S2). The lowest energy configuration is shown in Fig. 2a, in which the interfacial Se and Te are in the hollow sites. The stacking order is the same as the one for MnBi<sub>2</sub>Te<sub>4</sub> monolayer on In<sub>2</sub>Se<sub>3</sub><sup>71</sup>, which shows up for all MAT bilayers on In<sub>2</sub>Se<sub>3</sub>. Table I summarizes the stability of the two magnetic states for MAT bilayers on In<sub>2</sub>Se<sub>3</sub> monolayer in different polarization states. One can see that for all the MAT bilayers the IMCs remain AFM when the polarization is pointing toward the interface, but become FM as the polarization is reversed. The trend is independent of the vdW functionals/methods (Table S3). Below we focus on the electronic structure of MnBi<sub>2</sub>Te<sub>4</sub> bilayer on In<sub>2</sub>Se<sub>3</sub> monolayer, i.e., MnBi<sub>2</sub>Te<sub>4</sub>-2L/In<sub>2</sub>Se<sub>3</sub>, which are shown in Figs. 2b-d. Those for all other MAT systems are shown in Figs. S4-S6 since they show pretty much the same trend as MnBi<sub>2</sub>Te<sub>4</sub>-2L/In<sub>2</sub>Se<sub>3</sub>. The Fermi level is located in the band gap for the AFM state. Whereas for the FM state, the conduction band of In<sub>2</sub>Se<sub>3</sub> is shifted down into the valence band of MnBi<sub>2</sub>Te<sub>4</sub>-2L such that the Fermi level is crossing the valence band of the latter. This feature favors interfacial charge transfer. Fig. 2d depicts the differential charge density for the two magnetic states, which indicates that there is almost negligible interfacial charge transfer between the MnBi<sub>2</sub>Te<sub>4</sub>-2L and In<sub>2</sub>Se<sub>3</sub> for the AFM state. In contrast, the charge transfer is much more significant for the FM state than that for the AFM state. A close inspection finds that the charge density on the Mn atoms in the interfacial layer becomes positive. This confirms the picture of hole doping over this layer and opens up the  $e_g^\uparrow - \{p \dots p\} - e_g^\uparrow$  hopping channel. Consequently, the FM state becomes energetically favorable for this type of band structure. Thus, the FE In<sub>2</sub>Se<sub>3</sub> monolayer fits the criterion for a substrate that gives switchable band alignments between

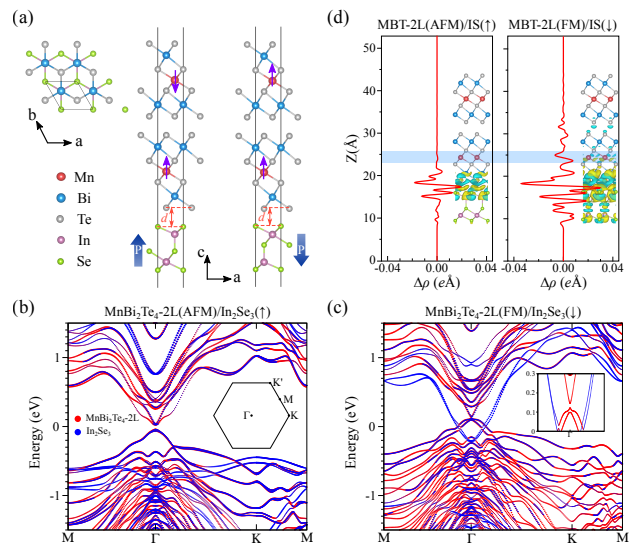


FIG. 2. Ferroelectric control of AFM-to-FM transition in MnBi<sub>2</sub>Te<sub>4</sub> bilayers. (a) Geometric structures of MnBi<sub>2</sub>Te<sub>4</sub>-2L/In<sub>2</sub>Se<sub>3</sub> heterostructures. Left panel shows the top view of the lowest energy configuration. Middle and right panels show the side view of the structures with different polarizations. The thin purple arrows denote spins of the Mn ions. While the thick blue arrows denote polarizations of the FE substrate. (b, c) Band structures for the two states in (a), respectively, i.e., MnBi<sub>2</sub>Te<sub>4</sub>-2L(AFM)/In<sub>2</sub>Se<sub>3</sub>(↑) and MnBi<sub>2</sub>Te<sub>4</sub>-2L(FM)/In<sub>2</sub>Se<sub>3</sub>(↓). (d) Planar-averaged differential charge density  $\Delta\rho(z)$  for the two states shown in (b) and (c). The insets show the density contour at 0.00015 e/Å<sup>3</sup>. Here, abbreviations (MBT-2L(AFM)/IS(↑) and MBT-2L(FM)/IS(↓)) are used by incorporating the IMCs of the MnBi<sub>2</sub>Te<sub>4</sub>-2L and the polarization states of In<sub>2</sub>Se<sub>3</sub> for simplicity.

type-II and type-III with MnBi<sub>2</sub>Te<sub>4</sub>-2L. Moreover, the trend that the charge transfer mainly happened to the interfacial layer also suggests that the spin-flipping accompanied by the AFM-FM transition takes place to the interfacial MnBi<sub>2</sub>Te<sub>4</sub> layer. For the trilayers and quadrilayers, our calculations find the same trend in the spin-flipping as the bilayers (Figs. S7 and S8).

On the other hand, the interface has a significant impact on the polarization states of the FE In<sub>2</sub>Se<sub>3</sub> monolayer by introducing a coupling between its polarizations and the local dipoles of MAT. This coupling breaks the symmetry of the two polarization states, that is, it gives rise to asymmetric barrier heights for the two polarization states. Fig. 3a shows that the state with the polarizations pointing toward the MnBi<sub>2</sub>Te<sub>4</sub> bilayer has a barrier height of about 152 meV ( $\Delta G^T$ ), which is about 68 meV lower than the one with polarizations pointing away from the interface ( $\Delta G^A$ ). Therefore, the critical electric fields needed to flip the polarizations for the former ( $E^T$ ) is smaller than that for the latter ( $E^A$ ), i.e.,  $E^T < E^A$ .

The asymmetric barrier heights along with the unique polarization-dependent IMCs allow designing ferroelec-

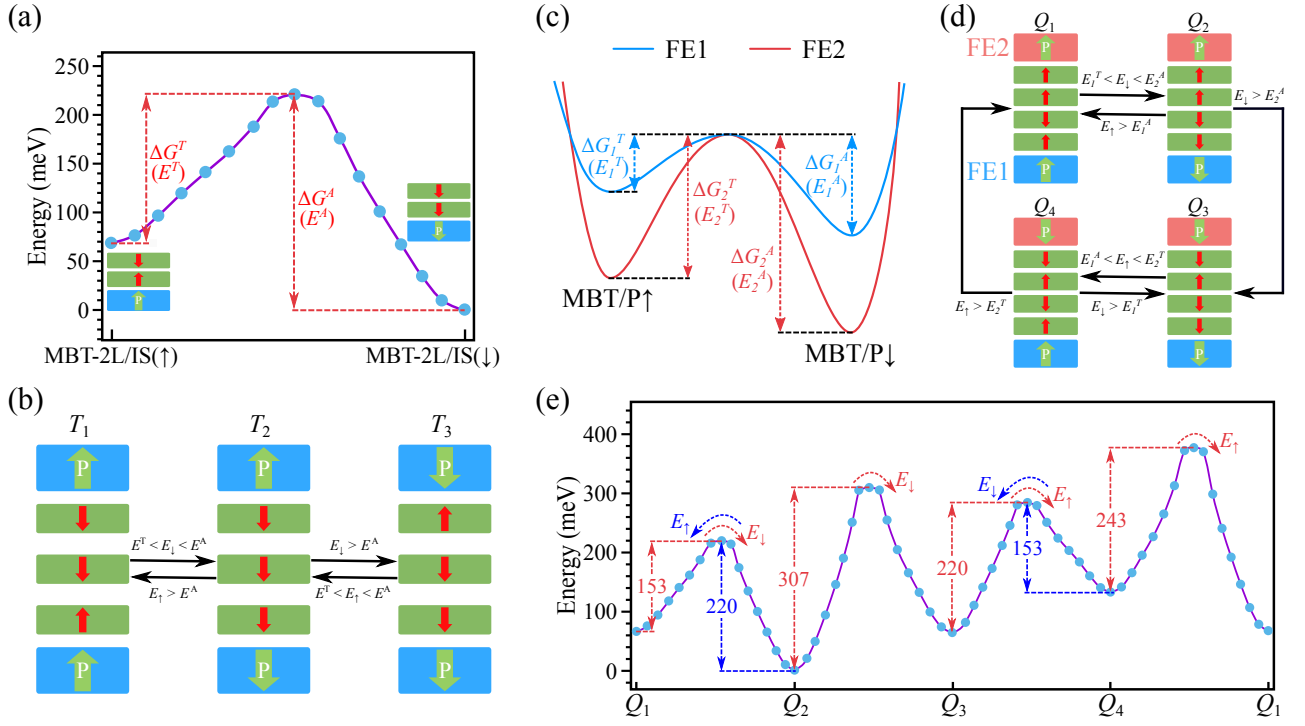


FIG. 3. Magnetic multistates in  $\text{MnBi}_2\text{Te}_4$  thin films. (a) Kinetic pathway of the FE phase transforming in  $\text{MnBi}_2\text{Te}_4\text{-2L}/\text{In}_2\text{Se}_3$  (abbreviated as MBT-2L/IS). Interface effects lead to asymmetric barrier heights for the two polarization states, which are labelled as  $\Delta G^T$  and  $\Delta G^A$  as the polarization point toward and away from the interface, respectively. Correspondingly, the critical electric fields are labelled as  $E^T$  and  $E^A$ , respectively. (b) Triple magnetic states in  $\text{In}_2\text{Se}_3/\text{MnBi}_2\text{Te}_4\text{-3L}/\text{In}_2\text{Se}_3$  and schematic FE transforming by controlling the external electric field.  $E_\uparrow$  ( $E_\downarrow$ ) represents the external electric fields along the  $z$  ( $-z$ ) axis. (c) Requirement of energy barriers of the two different FE layers for quadruple magnetic states in sandwich structure FE1/MBT-4L/FE2,  $\Delta G_1^T < \Delta G_1^A < \Delta G_2^T < \Delta G_2^A$ .  $\Delta G_1^T$  and  $\Delta G_1^A$  are for one FE layer (FE1), which is colored in blue. Critical electric fields needed to overcome these barriers are denoted as  $E_1^T$  and  $E_1^A$ , respectively.  $\Delta G_2^T$  and  $\Delta G_2^A$  are for the other layer (FE2) colored in red, for which the critical fields are  $E_2^T$  and  $E_2^A$ , respectively. (d) Schematic illustration of quadruple magnetic states in FE1/ $\text{MnBi}_2\text{Te}_4\text{-4L}/\text{FE2}$  and transforming between the states under electric fields. (e) Kinetic pathways of the quadruple states in  $\text{In}_2\text{Sse}_2/\text{MBT-4L}/\text{In}_2\text{Se}_3$  during FE transforming. The convention of labeling spins of the  $\text{Mn}^{+2}$  ions and the polarizations of  $\text{In}_2\text{Se}_3$  is the same as in Fig. 2.

trically switchable magnetic multistates for MAT multilayers. We illustrate the concept in  $\text{MnBi}_2\text{Te}_4$  trilayers and quadrayers, i.e.,  $\text{MnBi}_2\text{Te}_4\text{-3L}$  and  $\text{MnBi}_2\text{Te}_4\text{-4L}$ . We first sandwich  $\text{MnBi}_2\text{Te}_4\text{-3L}$  in between two  $\text{In}_2\text{Se}_3$  layers (Fig. 3b). Suppose that both the top and bottom  $\text{In}_2\text{Se}_3$  layers have up polarizations, which can be achieved by applying external electric fields anyway. According to the polarization dependent IMCs discussed above, spins in the  $\text{MnBi}_2\text{Te}_4$  layer next to the top  $\text{In}_2\text{Se}_3$  layer will be flipped so that it will be ferromagnetically coupled with the underneath  $\text{MnBi}_2\text{Te}_4$  layer. We label this magnetic state as  $T_1$ . Then one can apply an electrical field  $E_\downarrow$  antiparallel to the  $z$  axis that is larger than the critical field overcoming  $\Delta G^T$  but smaller than the critical field required to overcome  $\Delta G^A$ , i.e.,  $E^T < E_\downarrow < E^A$ . As a result, the polarizations in the bottom layer will be reversed while those in the top layer will remain unchanged. Then, the magnetization of the bottom  $\text{MnBi}_2\text{Te}_4$  layer will be flipped to be ferromagnetically coupled with the adjacent  $\text{MnBi}_2\text{Te}_4$  layer, i.e.,  $T_2$  in Fig. 3b. Further increasing

the electric field such that  $E_\downarrow > E^A$  will also drive the polarizations of the top  $\text{In}_2\text{Se}_3$  layer to be flipped. Correspondingly, the magnetizations of the top  $\text{MnBi}_2\text{Te}_4$  layer will be flipped, for which the magnetic state is labelled as  $T_3$ . Now, an electric field along the  $z$  axis, i.e.,  $E_\uparrow$ , will first force the polarization of the bottom  $\text{In}_2\text{Se}_3$  to be reversed when  $E^T < E_\uparrow < E^A$ . As a result, the system will flow into  $T_2$ . Further enhancing  $E_\uparrow$  to the level that  $E_\uparrow > E^A$  will drive the system back into  $T_1$ . So the whole system have triple magnetic states, which can be ferroelectrically controlled. Likewise, sandwiching thicker films than triple layers by the same FE layers also gives rise to triple magnetic states.

More magnetic states can be obtained by sandwiching the MAT thin films in between two different FE layers with a special combination of the barrier heights. Such a combination requires that the highest barrier for one FE monolayer should be lower than the lowest barrier for the other FE layer. We depict the barrier heights for the two different FE layers in Fig 3c,  $\Delta G_1^T$  and  $\Delta G_1^A$  are for one

TABLE I. Energy difference between the interlayer FM and AFM states for freestanding MAT bilayers and their bilayers supported by  $\text{In}_2\text{Se}_3$  monolayer in different polarization states (denoted by arrows).  $\Delta E = E_{FM} - E_{AFM}$ ,  $E_{FM}$  ( $E_{AFM}$ ) represents the total energy of the FM (AFM) state.

Systems	$\Delta E$ [meV/(Mn pair)]	IMCs
MnBi <sub>2</sub> Te <sub>4</sub> -2L	0.21	AFM
MnBi <sub>2</sub> Te <sub>4</sub> -2L/ $\text{In}_2\text{Se}_3$ ( $\uparrow$ )	0.22	AFM
MnBi <sub>2</sub> Te <sub>4</sub> -2L/ $\text{In}_2\text{Se}_3$ ( $\downarrow$ )	-0.16	FM
MnSb <sub>2</sub> Te <sub>4</sub> -2L	0.39	AFM
MnSb <sub>2</sub> Te <sub>4</sub> -2L/ $\text{In}_2\text{Se}_3$ ( $\uparrow$ )	0.36	AFM
MnSb <sub>2</sub> Te <sub>4</sub> -2L/ $\text{In}_2\text{Se}_3$ ( $\downarrow$ )	-0.40	FM
MnBi <sub>4</sub> Te <sub>7</sub> -2L	0.03	AFM
MnBi <sub>4</sub> Te <sub>7</sub> -2L/ $\text{In}_2\text{Se}_3$ ( $\uparrow$ )	0.03	AFM
MnBi <sub>4</sub> Te <sub>7</sub> -2L/ $\text{In}_2\text{Se}_3$ ( $\downarrow$ )	-0.01	FM
MnSb <sub>4</sub> Te <sub>7</sub> -2L	0.06	AFM
MnSb <sub>4</sub> Te <sub>7</sub> -2L/ $\text{In}_2\text{Se}_3$ ( $\uparrow$ )	0.09	AFM
MnSb <sub>4</sub> Te <sub>7</sub> -2L/ $\text{In}_2\text{Se}_3$ ( $\downarrow$ )	-0.04	FM

FE layer (FE1), to which the corresponding critical electric fields are  $E_1^T$  and  $E_1^A$ , respectively. Whereas  $\Delta G_2^T$  and  $\Delta G_2^A$  are for the other layer colored in red (FE2), for which the critical fields are  $E_2^T$  and  $E_2^A$ , respectively. In the case that  $\Delta G_1^T < \Delta G_1^A < \Delta G_2^T < \Delta G_2^A$ , i.e.,  $E_1^T < E_1^A < E_2^T < E_2^A$ , a layer-by-layer flipping mechanism for the FE contacts can be achieved by properly controlling the electric field. As a result, one can have quadruple magnetic states based on the polarization-dependent IMCs in MAT heterostructures (Fig. 3d). Our calculations find that the barrier heights of  $\text{In}_2\text{Se}_3$  and  $\text{In}_2\text{SSe}_2$  monolayers fit the above requirement for the quadruple magnetic states. Specifically, we obtain 245 meV ( $\Delta G_2^T$ ) and 308 meV ( $\Delta G_2^A$ ) for  $\text{In}_2\text{SSe}_2$  with polarizations pointing toward and away from the  $\text{MnBi}_2\text{Te}_4$  layer (see Figs. S9 and S10), respectively, which are larger than those of  $\text{In}_2\text{Se}_3$  (see Fig. 3a, 152 meV for  $\Delta G_1^T$  and 220 meV for  $\Delta G_1^A$ ). In Fig. 3e, we show the kinetic pathway of transforming the polarization states, which suggests that the quadruple states are ferroelectrically switchable.

The ferroelectrically tunable magnetic multistates give rise to a variety of distinct topological properties the MAT thin films. We perform calculations of the Chern number ( $C$ ) for the  $\text{MnBi}_2\text{Te}_4$  multilayers with the magnetic states show in Figs. 2 and 3. For the bilayer systems, the topological properties of  $\text{MnBi}_2\text{Te}_4$  remain unchanged upon interfacing, i.e.,  $C = 1$  for the FM state and  $C = 0$  for the AFM state, which is also supported by the results of edge states (Figs. S11 and S12). For  $\text{MnBi}_2\text{Te}_4$ -3L, we have  $C = 0, -1$ , and  $0$  for  $T_1, T_2$ , and  $T_3$ , respectively. Whereas for  $\text{MnBi}_2\text{Te}_4$ -4L, there are three Chern numbers for the quadruple states, i.e.,  $1, 0$ , and  $-1$ . Table II summarizes the Chern numbers for the studied  $\text{MnBi}_2\text{Te}_4$  thin films. We expect that such a

TABLE II. Chern number ( $C$ ) for  $\text{MnBi}_2\text{Te}_4$  multilayers with different magnetic states. Arrows denote the magnetizations on Mn ions.

Systems	IMCs	$C$
$\text{MnBi}_2\text{Te}_4$ -2L	M <sub>1</sub> ( $\uparrow\downarrow$ )	0
	M <sub>2</sub> ( $\downarrow\downarrow$ )	-1
$\text{MnBi}_2\text{Te}_4$ -3L	T <sub>1</sub> ( $\downarrow\downarrow\uparrow$ )	0
	T <sub>2</sub> ( $\downarrow\downarrow\downarrow$ )	-1
	T <sub>3</sub> ( $\uparrow\downarrow\downarrow$ )	0
$\text{MnBi}_2\text{Te}_4$ -4L	Q <sub>1</sub> ( $\uparrow\uparrow\downarrow\uparrow$ )	1
	Q <sub>2</sub> ( $\uparrow\uparrow\downarrow\downarrow$ )	0
	Q <sub>3</sub> ( $\downarrow\downarrow\downarrow\downarrow$ )	-1
	Q <sub>4</sub> ( $\downarrow\uparrow\downarrow\uparrow$ )	0

ferroelectrically tunable multiplet for the Chern number may be seen in other MAT multilayers.

In conclusion, we have proposed to ferroelectrically tune the magnetism of MAT thin films using model and first-principles calculations. The scheme is based on the fact that the IMCs are strongly dependent on the occupation of  $d$ -orbitals of the  $\text{Mn}^{2+}$  ions. The variation in the occupation can be controlled by interfacing the films with a FE layer with appropriate band alignments. We have demonstrated the concept in MAT/ $\text{In}_2\text{Se}_3$  heterostructures by performing first-principles calculations. We find that the interfacing effect mainly has an impact on the interfacial MAT layer. Specifically, there is spin-flipping in the interfacial layer when polarizations of the  $\text{In}_2\text{Se}_3$  are reversed, which results in ferroelectrically switchable IMCs and an AFM-to-FM transition. On the other hand, the interfacing effect leads to asymmetric energy barrier heights, which means that different electric fields are needed to switch the polarizations for the two states. We further show that this physics can be used to build magnetic multistates in their sandwich structures. Our calculations suggest that triple and quadruple magnetic states with tunable Chern number can be obtained for  $\text{MnBi}_2\text{Te}_4$  thin films by sandwiching them in between appropriate FE layers. Our results will not only attract experimental interest in FE control of the magnetism and topological properties of MAT thin films, but also inspire designing novel magnetism in other 2D materials.

## Acknowledgments

We thank Haijun Zhang and Zhixin Guo for useful discussions. This work was supported by the National Natural Science Foundation of China (Grants No. 12174098, No. 11774084, No. U19A2090 and No. 91833302) and project supported by State Key Laboratory of Powder Metallurgy, Central South University, Changsha, China.

- \* [mxchen@hunnu.edu.cn](mailto:mxchen@hunnu.edu.cn)
- <sup>1</sup> B. Huang, G. Clark, E. Navarro-Moratalla, D. R. Klein, R. Cheng, K. L. Seyler, D. Zhong, E. Schmidgall, M. A. McGuire, D. H. Cobden, W. Yao, D. Xiao, P. Jarillo-Herrero, and X. Xu, *Nature* **546**, 270 (2017).
  - <sup>2</sup> C. Gong, Z. Li, H. Ji, A. Stern, Y. Xia, W. Bao, Y. Wang, Z. Q. Qiu, R. J. Cava, S. G. Louie, J. Xia, and X. Zhang, *Nature* **546**, 265 (2017).
  - <sup>3</sup> Z. Fei, B. Huang, P. Malinowski, W. Wang, T. Song, J. Sanchez, W. Yao, D. Xiao, X. Zhu, A. F. May, W. Wu, D. H. Cobden, J.-H. Chu, and X. Xu, *Nat. Mater.* **17**, 778 (2018).
  - <sup>4</sup> K. S. Burch, D. Mandrus, and J.-G. Park, *Nature* **563**, 47 (2018).
  - <sup>5</sup> C. Gong and X. Zhang, *Science* **363**, eaav4450 (2019).
  - <sup>6</sup> L. Wang, Y. Shi, M. Liu, A. Zhang, Y.-L. Hong, R. Li, Q. Gao, M. Chen, W. Ren, H.-M. Cheng, Y. Li, and X.-Q. Chen, *Nat. Commun.* **12**, 2361 (2021).
  - <sup>7</sup> J. Y. Ni, X. Y. Li, D. Amoroso, X. He, J. S. Feng, E. J. Kan, S. Picozzi, and H. J. Xiang, *Phys. Rev. Lett.* **127**, 247204 (2021).
  - <sup>8</sup> B. Huang, G. Clark, D. R. Klein, D. MacNeill, E. Navarro-Moratalla, K. L. Seyler, N. Wilson, M. A. McGuire, D. H. Cobden, D. Xiao, W. Yao, P. Jarillo-Herrero, and X. Xu, *Nat. Nanotechnol.* **13**, 544 (2018).
  - <sup>9</sup> R. Xu and X. Zou, *J. Phys. Chem. Lett.* **11**, 3152 (2020).
  - <sup>10</sup> S. Jiang, L. Li, Z. Wang, K. F. Mak, and J. Shan, *Nat. Nanotechnol.* **13**, 549 (2018).
  - <sup>11</sup> D. Soriano and M. I. Katsnelson, *Phys. Rev. B* **101**, 041402 (2020).
  - <sup>12</sup> Y. Lu, R. Fei, X. Lu, L. Zhu, L. Wang, and L. Yang, *ACS Appl. Mater. Interfaces* **12**, 6243 (2020).
  - <sup>13</sup> H.-X. Cheng, J. Zhou, C. Wang, W. Ji, and Y.-N. Zhang, *Phys. Rev. B* **104**, 064443 (2021).
  - <sup>14</sup> B. Yang, B. Shao, J. Wang, Y. Li, C. Yam, S. Zhang, and B. Huang, *Phys. Rev. B* **103**, L201405 (2021).
  - <sup>15</sup> S. Shen, Q. Wu, Y. Dai, B. Huang, and Y. Ma, *Phys. Rev. B* **104**, 064446 (2021).
  - <sup>16</sup> H. Tian, C. Xu, X. Li, Y. Yang, L. Bellaiche, and D. Wu, *Phys. Rev. B* **103**, 125426 (2021).
  - <sup>17</sup> P. Li, X.-S. Zhou, and Z.-X. Guo, *NPJ Comput. Mater.* **8**, 1 (2022).
  - <sup>18</sup> Q. Tong, F. Liu, J. Xiao, and W. Yao, *Nano Lett.* **18**, 7194 (2018).
  - <sup>19</sup> T. Song, Q.-C. Sun, E. Anderson, C. Wang, J. Qian, T. Taniguchi, K. Watanabe, M. A. McGuire, R. Stöhr, D. Xiao, T. Cao, J. Wrachtrup, and X. Xu, *Science* **374**, 1140 (2021).
  - <sup>20</sup> M. Akram, H. LaBollita, D. Dey, J. Kapteghian, O. Erten, and A. S. Botana, *Nano Lett.* **21**, 6633 (2021).
  - <sup>21</sup> M. Otrokov, I. Klimovskikh, H. Bentmann, D. Estyunin, A. Zeugner, Z. Aliev, S. Gaß, A. Wolter, A. Koroleva, A. Shikin, M. Blanco-Rey, M. Hoffmann, I. Rusinov, A. Vyazovskaya, S. Ereemeev, Y. Koroteev, V. Kuznetsov, F. Freyse, J. Sánchez-Barriga, and E. Chulkov, *Nature* **576**, 416 (2019).
  - <sup>22</sup> D. Zhang, M. Shi, T. Zhu, D. Xing, H. Zhang, and J. Wang, *Phys. Rev. Lett.* **122**, 206401 (2019).
  - <sup>23</sup> J. Li, Y. Li, S. Du, Z. Wang, B.-L. Gu, S.-C. Zhang, K. He, W. Duan, and Y. Xu, *Sci. Adv.* **5**, eaaw5685 (2019).
  - <sup>24</sup> Y. Gong, J. Guo, J. Li, K. Zhu, M. Liao, X. Liu, Q. Zhang, L. Gu, L. Tang, X. Feng, D. Zhang, W. Li, C. Song, L. Wang, P. Yu, X. Chen, Y. Wang, H. Yao, W. Duan, Y. Xu, S.-C. Zhang, X. Ma, Q.-K. Xue, and K. He, *Chin. Phys. Lett.* **36**, 076801 (2019).
  - <sup>25</sup> Y.-J. Hao, P. Liu, Y. Feng, X.-M. Ma, E. F. Schwier, M. Arita, S. Kumar, C. Hu, R. Lu, M. Zeng, Y. Wang, Z. Hao, H.-Y. Sun, K. Zhang, J. Mei, N. Ni, L. Wu, K. Shimada, C. Chen, Q. Liu, and C. Liu, *Phys. Rev. X* **9**, 041038 (2019).
  - <sup>26</sup> C. Liu, Y. Wang, H. Li, Y. Wu, Y. Li, J. Li, K. He, Y. Xu, J. Zhang, and Y. Wang, *Nat. Mater.* **19**, 522 (2020).
  - <sup>27</sup> Y. Deng, Y. Yu, M. Z. Shi, Z. Guo, Z. Xu, J. Wang, X. H. Chen, and Y. Zhang, *Science* **367**, 895 (2020).
  - <sup>28</sup> J.-Q. Yan, Q. Zhang, T. Heitmann, Z. Huang, K. Y. Chen, J.-G. Cheng, W. Wu, D. Vaknin, B. C. Sales, and R. J. McQueeney, *Phys. Rev. Materials* **3**, 064202 (2019).
  - <sup>29</sup> J. Ge, Y. Liu, J. Li, H. Li, T. Luo, Y. Wu, Y. Xu, and J. Wang, *Natl. Sci. Rev.* **7**, 1280 (2020).
  - <sup>30</sup> C. Hu, K. N. Gordon, P. Liu, J. Liu, X. Zhou, P. Hao, D. Narayan, E. Emmanouilidou, H. Sun, Y. Liu, H. Brawer, A. P. Ramirez, L. Ding, H. Cao, Q. Liu, D. Dessau, and N. Ni, *Nat. Commun.* **11**, 97 (2020).
  - <sup>31</sup> Z. Li, J. Li, K. He, X. Wan, W. Duan, and Y. Xu, *Phys. Rev. B* **102**, 081107 (2020).
  - <sup>32</sup> L. Zhou, Z. Tan, D. Yan, Z. Fang, Y. Shi, and H. Weng, *Phys. Rev. B* **102**, 085114 (2020).
  - <sup>33</sup> X. Wu, J. Li, X.-M. Ma, Y. Zhang, Y. Liu, C.-S. Zhou, J. Shao, Q. Wang, Y.-J. Hao, Y. Feng, E. F. Schwier, S. Kumar, H. Sun, P. Liu, K. Shimada, K. Miyamoto, T. Okuda, K. Wang, M. Xie, C. Chen, Q. Liu, C. Liu, and Y. Zhao, *Phys. Rev. X* **10**, 031013 (2020).
  - <sup>34</sup> B. Lian, Z. Liu, Y. Zhang, and J. Wang, *Phys. Rev. Lett.* **124**, 126402 (2020).
  - <sup>35</sup> S. Yang, X. Xu, Y. Zhu, R. Niu, C. Xu, Y. Peng, X. Cheng, X. Jia, Y. Huang, X. Xu, J. Lu, and Y. Ye, *Phys. Rev. X* **11**, 011003 (2021).
  - <sup>36</sup> H. Zhang, W. Yang, Y. Wang, and X. Xu, *Phys. Rev. B* **103**, 094433 (2021).
  - <sup>37</sup> Z. Zhang, N. Wang, N. Cao, A. Wang, X. Zhou, K. Watanabe, T. Taniguchi, B. Yan, and W.-b. Gao, *Nature Communications* **13**, 6191 (2022).
  - <sup>38</sup> S. Li, M. Gong, S. Cheng, H. Jiang, and X. C. Xie, “Dissipationless layertronics in axion insulator  $\text{MnBi}_2\text{Te}_4$ ,” (2022).
  - <sup>39</sup> R. C. Vidal, A. Zeugner, J. I. Facio, R. Ray, M. H. Haghighi, A. U. B. Wolter, L. T. Corredor Bohorquez, F. Caglieris, S. Moser, T. Figgemeier, T. R. F. Peixoto, H. B. Vasili, M. Valvidares, S. Jung, C. Cacho, A. Alfonso, K. Mehawat, V. Kataev, C. Hess, M. Richter, B. Büchner, J. van den Brink, M. Ruck, F. Reinert, H. Bentmann, and A. Isaeva, *Phys. Rev. X* **9**, 041065 (2019).
  - <sup>40</sup> A. Zeugner, F. Nietschke, A. U. B. Wolter, S. Gaß, R. C. Vidal, T. R. F. Peixoto, D. Pohl, C. Damm, A. Lubk, R. Hentrich, S. K. Moser, C. Fornari, C. H. Min, S. Schatz, K. Kißner, M. Ünzelmann, M. Kaiser, F. Scaravaggi, B. Rellinghaus, K. Nielsch, C. Hess, B. Büchner, F. Reinert, H. Bentmann, O. Oeckler, T. Doert, M. Ruck, and A. Isaeva, *Chemistry of Materials* **31**, 2795 (2019), <https://doi.org/10.1021/acs.chemmater.8b05017>.
  - <sup>41</sup> P. M. Sass, J. Kim, D. Vanderbilt, J. Yan, and W. Wu, *Phys. Rev. Lett.* **125**, 037201 (2020).

- <sup>42</sup> J.-Q. Yan, Y. H. Liu, D. S. Parker, Y. Wu, A. A. Aczel, M. Matsuda, M. A. McGuire, and B. C. Sales, *Phys. Rev. Materials* **4**, 054202 (2020).
- <sup>43</sup> M. M. Otrokov, I. P. Rusinov, M. Blanco-Rey, M. Hoffmann, A. Y. Vyazovskaya, S. V. Eremin, A. Ernst, P. M. Echenique, A. Arnau, and E. V. Chulkov, *Phys. Rev. Lett.* **122**, 107202 (2019).
- <sup>44</sup> Z. Zang, Y. Zhu, M. Xi, S. Tian, T. Wang, P. Gu, Y. Peng, S. Yang, X. Xu, Y. Li, B. Han, L. Liu, Y. Wang, P. Gao, J. Yang, H. Lei, Y. Huang, and Y. Ye, *Phys. Rev. Lett.* **128**, 017201 (2022).
- <sup>45</sup> H. Wang, D. Wang, Z. Yang, M. Shi, J. Ruan, D. Xing, J. Wang, and H. Zhang, *Phys. Rev. B* **101**, 081109 (2020).
- <sup>46</sup> Y. Han, S. Sun, S. Qi, X. Xu, and Z. Qiao, *Phys. Rev. B* **103**, 245403 (2021).
- <sup>47</sup> S. X. M. Riberolles, Q. Zhang, E. Gordon, N. P. Butch, L. Ke, J.-Q. Yan, and R. J. McQueeney, *Phys. Rev. B* **104**, 064401 (2021).
- <sup>48</sup> T. Murakami, Y. Nambu, T. Koretsune, G. Xiangyu, T. Yamamoto, C. M. Brown, and H. Kageyama, *Phys. Rev. B* **100**, 195103 (2019).
- <sup>49</sup> Y. Liu, L.-L. Wang, Q. Zheng, Z. Huang, X. Wang, M. Chi, Y. Wu, B. C. Chakoumakos, M. A. McGuire, B. C. Sales, W. Wu, and J. Yan, *Phys. Rev. X* **11**, 021033 (2021).
- <sup>50</sup> M. Du, J. Yan, V. R. Cooper, and M. Eisenbach, *Advanced Functional Materials* **31**, 2006516 (2021).
- <sup>51</sup> M. Garnica, M. M. Otrokov, P. C. Aguilar, I. I. Klimovskikh, D. Estyunin, Z. S. Aliev, I. R. Amiraslanov, N. A. Abdullayev, V. N. Zverev, M. B. Babanly, N. T. Mamedov, A. M. Shikin, A. Arnau, A. L. V. de Parga, E. V. Chulkov, and R. Miranda, *npj Quantum Materials* **7**, 7 (2022).
- <sup>52</sup> M. Liu, C. Lei, H. Kim, Y. Li, L. Frammolino, J. Yan, A. H. Macdonald, and C.-K. Shih, *Proceedings of the National Academy of Sciences* **119**, e2207681119 (2022).
- <sup>53</sup> S. Du, P. Tang, J. Li, Z. Lin, Y. Xu, W. Duan, and A. Rubio, *Phys. Rev. Research* **2**, 022025 (2020).
- <sup>54</sup> J. Xiao and B. Yan, *2D Materials* **7**, 045010 (2020).
- <sup>55</sup> H. Fu, C.-X. Liu, and B. Yan, *Sci. Adv.* **6**, eaaz0948 (2020).
- <sup>56</sup> G. Kresse and J. Furthmüller, *Phys. Rev. B* **54**, 11169 (1996).
- <sup>57</sup> W. Ding, J. Zhu, Z. Wang, Y. Gao, D. Xiao, Y. Gu, Z. Zhang, and W. Zhu, *Nat. Commun.* **8**, 14956 (2017).
- <sup>58</sup> Y. Zhou, D. Wu, Y. Zhu, Y. Cho, Q. He, X. Yang, K. Herrera, Z. Chu, Y. Han, M. C. Downer, H. Peng, and K. Lai, *Nano Lett.* **17**, 5508 (2017).
- <sup>59</sup> C. Cui, W.-J. Hu, X. Yan, C. Addiego, W. Gao, Y. Wang, Z. Wang, L. Li, Y. Cheng, P. Li, X. Zhang, H. N. Alshareef, T. Wu, W. Zhu, X. Pan, and L.-J. Li, *Nano Lett.* **18**, 1253 (2018).
- <sup>60</sup> P. E. Blöchl, *Phys. Rev. B* **50**, 17953 (1994).
- <sup>61</sup> G. Kresse and D. Joubert, *Phys. Rev. B* **59**, 1758 (1999).
- <sup>62</sup> S. Grimme, J. Antony, S. Ehrlich, and H. Krieg, *J. Chem. Phys.* **132**, 154104 (2010).
- <sup>63</sup> S. Grimme, *J. Comput. Chem.* **27**, 1787 (2006).
- <sup>64</sup> J. Klimeš, D. R. Bowler, and A. Michaelides, *J. Phys.: Condens. Matter* **22**, 022201 (2009).
- <sup>65</sup> J. c. v. Klimeš, D. R. Bowler, and A. Michaelides, *Phys. Rev. B* **83**, 195131 (2011).
- <sup>66</sup> S. L. Dudarev, G. A. Botton, S. Y. Savrasov, C. J. Humphreys, and A. P. Sutton, *Phys. Rev. B* **57**, 1505 (1998).
- <sup>67</sup> G. Henkelman, B. P. Uberuaga, and H. Jónsson, *J. Chem. Phys.* **113**, 9901 (2000).
- <sup>68</sup> G. Henkelman and H. Jónsson, *J. Chem. Phys.* **113**, 9978 (2000).
- <sup>69</sup> A. A. Mostofi, J. R. Yates, Y.-S. Lee, I. Souza, D. Vanderbilt, and N. Marzari, *Comput. Phys. Commun.* **178**, 685 (2008).
- <sup>70</sup> Q. Wu, S. Zhang, H.-F. Song, M. Troyer, and A. A. Soluyanov, *Comput. Phys. Commun.* **224**, 405 (2018).
- <sup>71</sup> F. Xue, Z. Wang, Y. Hou, L. Gu, and R. Wu, *Phys. Rev. B* **101**, 184426 (2020).